Setting up a methodology to distinguish between green oranges and leaves using hyperspectral imaging

Irina Torres[a], María-Teresa Sánchez[a,]*, Byoung-Kwan Cho[b], Ana Garrido-Varo[c], Dolores Pérez-Marín[c,]*

[a] *Department of Bromatology and Food Technology, College of Agriculture and Forestry Engineering (ETSIAM), University of Cordoba, Campus of Rabanales, 14071 Córdoba, Spain.*

[b] *Department of Biosystems Machinery Engineering, College of Agricultural and Life Science, Chungnam National University, 220 Gung-dong, Yuseong-gu, Daejeon 305-764, Republic of Korea*

[c] *Department of Animal Production, College of Agriculture and Forestry Engineering (ETSIAM), University of Cordoba, Campus of Rabanales, 14071 Córdoba, Spain.*

*Corresponding authors. Tel.: +34 957 212576; fax: 34 957 212000

E-mail addresses: teresa.sanchez@uco.es (M.T. Sánchez) or dcperez@uco.es (D. Pérez-Marín).

ABSTRACT

The estimation of green citrus fruit yield is a key parameter for growers and the industry. The early estimation of orange yield at the immature green stage could influence the future market price and allow producers to plan the harvest in advance, thus reducing costs. This research can be considered as a preliminary step for designing low-cost spectral cameras capable of being mounted on unmanned aerial vehicles (UAVs) to estimate orange yield and defects. Images were acquired from oranges and leaves from an orchard in Jeju island (Jeju, Republic of Korea), using two hyperspectral reflectance imaging systems, one working in the range 400–1000 nm (visible/near infrared, Vis/NIR) and the other between 900–2500 nm (short-wave infrared, SWIR). The main objective of the research was to set up a methodology to select the relevant bands - from the two spectral ranges studied - to distinguish between green oranges and leaves and to detect defects, which will allow citrus yield to be estimated. Analysis of variance (ANOVA) and principal component analysis (PCA) were used to select the key wavelengths for this purpose; next, a band ratio coupled with a simple thresholding method was applied. This study showed that the Vis/NIR hyperspectral imaging correctly classified 96.97% and 92.93% of the pixels, respectively, to distinguish between green oranges and leaves and to detect defects, while with the SWIR system, the percentage of pixels correctly classified for these two objectives were 74.79% and 89.31%, respectively. These results confirm that it is possible to use a low number of wavelengths to estimate harvest yield in oranges, which could pave the way for the future development of low-cost and low-weight equipment for the detection of green and sound fruit.

Keywords: Orange; Harvest yield; Defect detection; Hyperspectral and multispectral imaging

1. Introduction

The citrus sector is one of the most dynamic and important agricultural sectors. This sector is of considerable economic value to the countries of the Mediterranean Basin, China, Brazil, the United States and Southeast Asia (Republic of Korea), the main producers of citrus fruit, in general, and of oranges in particular (FAO, 2017).

In the light of the economic importance of the orange on the international market, it is of particular interest to obtain an estimate of the crop yield prior to harvesting, which usually takes place when the fruits are of the same green colour as the leaves (Obenland et al., 2009). In oranges, the fruits often reach physiological maturity and present excellent eating quality while the peel is still green. Post-harvest de-greening practices are used to speed up the fruit colour change and to make the fruit more acceptable for marketing, since a shiny, yellow peel is what the market demands (Porat, 2008).

Therefore, tools are needed to identify these green fruits on-tree, to make possibly decision on harvesting and to optimize the process, so that fruits of the highest quality are picked in keeping with their subsequent industrial use.

Currently, the indexes used to determine quality in oranges are colour intensity and uniformity, firmness, size, shape, quality of flavour, lack of decay and lack of defects including physical damage (abrasions and bruising), skin blemishes and discoloration, as well as insect damage (Arpaia and Kader, 1999): this last quality index is one of the most influential factors on yield in fresh oranges (Leemans and Destain, 2004; Li et al., 2011).

These days, the large-scale measurement of these production and quality indicators still constitutes a major difficulty for producers. On the one hand, it is believed that drones with a sensing unit may be used in the near future to achieve this aim due to the rise in their popularity for agricultural applications; on the other, hyperspectral imaging (HSI) and multispectral imaging (MSI) are two emerging techniques which could be used for this purpose, due to their ability to acquire both spectral and spatial information and thus assess quality indexes in agricultural products (Dale et al., 2013).

As far as the present authors are aware, only two published studies have used HSI technology to distinguish between green oranges and leaves on-tree. In the first, Kane and Lee (2007) used an InGaAs camera with a spectral range of 900 to 1700 nm to identify green oranges in the field. They applied a combination of three different spectral band images to identify the green orange and achieved an accuracy of 84.5% in terms of correctly classified pixels. In the other, Okamoto and Lee (2009) using a CCD hyperspectral camera in the 369–1042 nm range applied stepwise forward variable selection method and linear discriminant analysis was then developed with selected variables - between 10 and 14 - to identify green citrus fruits in the field at different stages, with detection accuracies for complete fruit ranging between 80 to 89%.

As regards detecting external defects in oranges, a number of studies have been published to date, all of which were carried out under laboratory conditions, with the aim of selecting the optimal wavelengths for this application with a multispectral system (Li et al. 2011; Bulanon et al., 2013; Lorente et al., 2013; Li et al., 2016).

In addition, the recent development of small-sized hyperspectral and multispectral sensors has enabled them to be attached to UAVs in order to obtain images with a high spectral and spatial resolution (Dale et al., 2013). The use of multispectral instead of hyperspectral cameras would reduce the cost of the system and would speed up the data analysis (Kim et al., 2011), although it would be necessary to make a prior selection of the optimal spectral bands for each particular objective.

Likewise, it is important to consider that the HSI measurement devices can affect the quality of the image data, so the selection of the instrument and the wavebands play an important role in optimising the performance of the application (Kim et al., 2011).

Most of the research carried out using multi and hyperspectral cameras to measure quality attributes (sweetness and acidity, firmness, stage of maturity or detection of defects) in fruit and vegetables have been carried out in the Vis/NIR region (400–1000 nm) (Kim et al., 2011; Li et al., 2018), although other studies have also used instruments in the SWIR range (1000–2500 nm) (Gowen et al., 2007). This spectral range is of particular interest to the citrus sector, since it not only allows us to differentiate between specific areas of the fruit (i.e. for detecting defects), but also includes the most suitable wavelengths for measuring the chemical parameters, such as soluble solid content and acidity (Williams, 2001).

Thus, given the numerous options available in terms of equipment, the successful implementation of hyperspectral or multispectral reflectance technology *in-situ* for crop yield estimation requires the instrument to be selected previously and the correct waveband combination to be found for this specific application. Although this aspect is hugely relevant when designing low-cost and low-weight cameras, to our knowledge there are no reports in the literature regarding the comparison between Vis/NIR and SWIR HSI systems to identify green citrus fruits and to pick out defective ones.

The objective of this work was to evaluate – at the laboratory scale – two line-scan hyperspectral reflectance imaging systems working in the Vis/NIR and SWIR ranges, respectively, to estimate the crop yield of oranges based on the distinction between green oranges and leaves and the detection of external defects (abrasions and bruising, skin blemishes and discoloration) in the oranges. The performance of these two systems was also compared and the optimal wavelengths were selected for the further development of a low-cost and low-weight MSI system which could be mounted on drones.

2. Material and methods

2.1. Sampling

The oranges and leaves were obtained from an orchard in Jeju island (Jeju, Republic of Korea) in autumn 2017.

For the first of the objectives – to differentiate green oranges from leaves – 20 leaves and 24 green oranges were placed in plastic bags and immediately taken to the laboratory. In the case of the leaves, wet tissues were put into the bags to maintain the moisture content of the leaves. Once in the laboratory, images of the leaves and green oranges were taken. Next, a set made up of 5 samples of green oranges together with their leaves was measured to validate the model obtained.

For the second objective – to identify oranges with defects – a total of 20 oranges with some external defects (abrasions and bruising, skin blemishes and discoloration) were measured.

Although the number of samples available in this study could appear to be limited, it is enough to evaluate the potential of the developed methodology.

2.2. Hyperspectral imaging systems and image acquisition

Two laboratory-based push-broom Vis/NIR and SWIR systems were used to obtain the hyperspectral images of oranges and leaves. Details of both imaging systems are given in Table 1.

The Vis/NIR system was made up of an Electron Multiplying Charge Coupled Device (EMCCD) camera (Luca R DL-604M, 14-bit, Andor Technology, South Windsor, CT, USA), a C-mount objective lens (F1.4 28-mm compact lens, Schneider Optics, Hauppauge, NY, USA), a line scan imaging spectrograph (Vis/NIR, Headwall photonics, Fitchburg, MA, USA) and halogen light sources (4 x 2 sets of 100 W) at a 45° angle to the sample. Next, in order to reduce specular reflection, the system was equipped with a glass rotating polarizer available for Vis/NIR region. The nominal reflectance range was approximately 400 to 1000 nm, with a spectral resolution of 4.7 nm. In order to capture the actual shape of samples by keeping the pixels shape nearly square, the number of lines was set at 1200 and 1080, with the distance between the lines set at 0.250 and 0.278 mm for the oranges and the leaves, respectively. Spectral data was stored on a 1200 x 502 x 128 hypercube for the oranges and a 1080 x 502 x 128 hypercube for the leaves.

For the SWIR system, a 384 x 256 pixel InGaAs camera (MCT, Headwall Photonics, Fitchburg, MA, USA) with spectrograph (Headwall Photonics, Fitchburg MA, USA) and C-mount 1.4/25 mm focal length lens (Navitar, Inc., Rochester, NY, USA) was used to collect images over a wavelength range of 900 to 2500 nm with 6 nm spectral resolution. The illumination for reflectance imaging was provided by six tungsten halogen lamps (100 W) connected by optical fibres and set up at a 45º angle. Line-by-line images were collected by a conveyor unit enable to cover the spatial shape of the samples; it was set to move at a 0.328 mm/scan for oranges and a 0.364 mm/scan for leaves.

To obtain the imaging using each hyperspectral system, 3 oranges were placed on a tray (30 x 12.5 cm) in a single row, while for the leaves, a batch of four samples on a 30 x 14 cm tray was imaged with a single take. The sound, green orange samples were arranged so that the stems pointed upwards, whereas the defective oranges were manually arranged to present the defects for imaging. As for the leaves, these were arranged with the adaxial side facing upwards.

Tablet movement was controlled by the step interval and the number of steps. Visual Basic 6.0 (Microsoft, Seattle, WA, USA) was used to run the HSI system and to control both conveyor and motor speed (0.25 mm/s for Vis/NIR and 8 mm/s for SWIR), instantaneous field of view (IFOV) and exposure time (Table 1). The two-dimensional spectral and spatial data were captured by the EMCCD and InGaAs cameras and stored in raw format as a 3D hypercube (two spatial and one spectral dimension), which comprised each spatial location and spectral information at each wavelength (λ).

Due to the heterogeneous intensities of the light source across the whole wavelength range, reflectance calibration was performed before each measurement by taking dark and white reference images. The dark reference was obtained by covering the camera lens with a black cap (0% reflectance) and the white reference by using white Teflon (99% reflectance). The reflectance value (R) of the raw images (R_0) was calculated using the dark (D) and white (W) reference and taking into account the correction factor for the reference panel (C) as in following equation (Kim et al., 2001):

$$R = \frac{R_0 - D_i}{W_i - D_i} \, x \, C_i$$

where *i* is the pixel index (i = 1, 2, 3, …, n) and *n* is the total number of pixels and the correction factor (C) of 1 was used.

2.3. Image processing and analysis

The steps followed in the full procedure of image processing and analysis for both instruments are shown in Figure 1. To achieve this aim, Matlab software (version 2015a, The Mathworks, Natick, MA, USA) was used. In the case of the SWIR system, the spectral range used was 900 to 1900 nm due to the fact that there was no signal beyond this wavelength.

After reflectance correction, the region of interests (ROIs) for sound green oranges and leaves were manually selected using a reflectance image. The spectra of all pixels in each ROI was extracted and averaged to obtain the mean intensity value for each wavelength.

For the identification of oranges, the selection of the most significant wavelengths for the distinction of green oranges and leaves was based on F-values of the analysis of variance (ANOVA) between the two groups (i.e. green oranges *versus* leaves). The higher the F-value, the more statistically significant the mean separation between groups (Neter et al., 1996; Cho et al., 2013). In the case that only one wavelength could be extracted from the ANOVA analysis, PCA was also used to determine the other wavelength needed to obtain the ratio. Thus, the wavebands which presented the greatest difference were used in the application of the ratio image.

For the detection of defects, PCA was used for all the hyperspectral data sets, including the spatial and spectral dimensions. This algorithm reduces the spectral dimensionality, since it converts the huge amount of data from the hypercube into a limited set of scores and loadings. In this work, the PC images and the loading vectors for the first three principal components (PC1, PC2, PC3) were used to select robust wavelengths for the proposed objectives; for this goal, the mean centre was performed as a pre-processing method (Wise et al., 2006).

Prior to using the PCA, a binary mask image was generated in order to avoid interferences from background that could decrease the accuracy of the method. To achieve this, the images at wavelengths 712.5 nm and 1065.11 nm were used for the segmentation for the Vis/NIR and SWIR hyperspectral images, respectively, since they showed the best contrast between the sample and the background. The background was removed by setting a simple threshold value ($R < 0.045$ for Vis/NIR and $R < 0.073$ SWIR) for these wavelengths, respectively, which was then applied to all the hypercubes.

Because the band-ratio can enhance the contrast between different regions (Vargas et al., 2005), two different band-ratios were used to distinguish between the green oranges and the leaves and to detect external defects in the oranges. The two-band ratio was performed as the following equation:

$$Q_{t/k} = \frac{R_t}{R_k}$$

where $Q_{t/k}$ represents a quotient of spectral reflectances, and R_t and R_k are the reflectance intensities at t nm and k nm.

The frequency histograms of the ratio values were recorded in order to select the optimal threshold values. Finally, the accuracy of the models was calculated as the percentage of correctly classified pixels.

To ensure the robustness of the models developed, their external validation was carried out. To achieve this, for differentiating between the leaves and the green oranges, the 5 samples of oranges attached to leaves were used, while to detecting the defects, 25% of the total defective samples (i.e. 5 fruits not used to develop the model) were randomly selected for validation.

3. Results and discussion

3.1. Spectral analysis

Representative mean reflectance spectra of green oranges and leaves after normalization, calculated from the pixel values of the ROIs for each system, are shown in Figure 2.

Fig. 2a shows the mean spectra obtained using the Vis/NIR system in the spectral region 400–1000 nm. Although the spectral patterns for both – green oranges and leaves- were fairly similar, in the green-yellow area of the spectrum (500~600 nm) the average reflectance obtained from the green oranges samples was higher than that obtained from the leaves. This makes sense, since in the visible range, the dominant process taking place is pigment absorption; in particular, the peak around 530 nm is due to β-carotene (Keşan et al., 2016). In addition, one dominant spectral feature observed in both spectra is the absorption of chlorophyll *a* at approximately 680 nm (Cho et al., 2013), whereas in the range between 900 and 1000 nm, corresponding to the water band (Williams, 2001), the oranges display lower intensity than the leaves.

The mean spectra obtained using the SWIR system in the spectral region 900–1900 is shown in Fig. 2b. As in the case of the Vis/NIR system, the characteristic shape of both spectra is very similar, with peaks and valleys in the same wavelengths. Here, the greatest difference in reflectance values occurred mainly around 1100 nm and 1400-1600 nm. These values were related to the molecular vibrations corresponding to the C–H and O–H bonds (Williams, 2001).

3.2. Optimal wavelengths selection to distinguish between green oranges and leaves

Figure 3 shows F-values for the ANOVA analysis between the two groups (i.e. green oranges *versus* leaves) for each wavelength and the two systems tested.

With the Vis/NIR system, the F-values of each waveband in the range 400–1000 nm obtained from the ANOVA analysis for distinguishing oranges and leaves are displayed in Fig. 3a. The highest F values were obtained for the bands 941.7 nm and 951.2 nm. Since these two bands were fairly close to each other, the band that yielded the highest

F-value was selected; in this case, the band 951.2 nm was chosen as one of the dominant bands. This wavelength is very close to one of those chosen (967.2 nm) by Okamoto and Lee (2009) to fulfil this objective using a sample group consisting of 3 varieties of green oranges. This band corresponds to water absorption, which is the main component in oranges (Williams, 2001).

Since only one wavelength could be extracted from the ANOVA analysis, PCA had to be used to determine the other wavelength needed to obtain the ratio.

It was visually determined that the PC2 image (with 1.07% of the explained variance) appeared to provide the best discrimination between green oranges and leaves. The PC2 weighting coefficients showed high positive values in the red region and negative values in the NIR region related to the O-H bond (Williams, 2001); the 698.2 nm wavelength, related to the absorption of chlorophyll *a,* was taken as the maximum, dominant wavelength (Cho et al., 2013).

Based on these results, the 698.2 nm and 951.2 nm bands, obtained from the PCA and ANOVA analyses, respectively, were selected for the MSI design. The raw and binary images, as well as the image obtained after the application of band ratio $R_{\lambda 698}$/ $R_{\lambda 951}$ and its corresponding frequency histogram, are shown in Fig. 4.

To obtain the global classification capacity of the model, this band ratio was applied to the validation set. The results indicated that for the $R_{\lambda 698}$/ $R_{\lambda 951}$ band ratio, the highest classification accuracy (96.97%) for oranges *versus* leaves was obtained using a threshold value of 1.00, which was obtained from the frequency histogram (Fig. 4d), in which two clearly differentiated populations can be observed, with an overlap between the intensity values of 0.90 and 1.00.

In the same way as in the Vis/NIR system, when using the SWIR system, the dominant bands were selected from the F-values of ANOVA between the groups of green oranges and leaves (Fig. 3b). The results showed that the wavelengths which gave rise to a more significant separation were 1165, 1259 and 1471 nm.

Since the purpose of this study was to minimize the number of spectral bands so that the measurement system to be developed would be as light weight, simple and economical as possible, only two of these wavelengths were selected, those whose ratio provided the greatest differentiation between leaves and fruits. Thus, from all the two-band combinations available, the ratio of wavebands at 1165 and 1471 nm ($R_{\lambda 1165}/ R_{\lambda 1471}$), which corresponded to the molecular bonds C-H and the molecular vibrations caused by O-H bonds**,** respectively (Williams, 2001), produced the clearest separation, as shown in Fig. 5. These wavelengths coincide with two of those selected by Kane and Lee (2007) for on-tree green citrus fruit identification**,** which is the only work with this objective found in the literature.

The validation results showed that by applying a simple threshold value (2.60), obtained from the frequency histogram (figure not shown), the classification accuracy was about 74.79%.

The accuracy obtained using the SWIR system was around 22% lower than that yielded with the Vis/NIR system. In Fig. 5, it can be seen that when applying the band-ratio to the image with the SWIR equipment, not only is there a less distinct separation between the leaf and the green orange than with the Vis/NIR system (Fig. 4c), but there is also an area in the centre of the fruit with less intensity which corresponds to the specular reflection caused by the geometry of the orange (Garrido-Novell et al., 2012). With the Vis/NIR system, this difference was reduced by using the polarizer, whose function is to reduce specular reflection in samples with curved or shiny surfaces; however, this was not possible with the SWIR system, as this accessory is not easily available for the SWIR spectral range. Thus, the problem is not the range of the camera used, but the lack of a polarizer to reduce the effect of specular reflection on the fruit.

3.3. Optimal wavelengths selection to detect external defects in oranges

Fig. 6 shows the score images and loadings plots for the first three PCs obtained in the calibration set of hyperspectral images of defective oranges after background removal using the Vis/NIR system. The first three PCs accounted for 99.92% of the explained variance, and it was found that the PCs above the third did not provide any useful information for detecting defects (data not shown). In the image corresponding to PC1 (96.37%), the areas of the oranges which especially stood out are those where, due to the spherical shape of fruit, higher intensities were produced because they were closer to the camera (Lee et al., 2008). Subsequent PC images represent other features ordered according to variations in spectral responses. In general terms, PC2 images exhibit the greatest contract between the sound and defective areas of the oranges, and so appear to have high discrimination power for identifying the defective areas**.** In PC3, the defects can be observed, and the stem of the fruit can clearly be seen, although no visual differences between these two features were recognized.

In addition, Fig. 6 also shows the loadings for the PC images (PC1–PC3) obtained from the hyperspectral images across the Vis/NIR region. The peaks and valleys show the dominant wavelengths, with maximums of 760 nm observed in PC1, 679 nm in PC2 and 665 nm in PC3, and minimums around 755 nm and 693 nm in PC2 and PC3, respectively, with no minimum of note observed in PC1. In view of these results, it can be stated that within the visible spectrum range, the red region and, in particular, those wavelengths related to the absorption of chlorophyll a, are predominant (Martínez-Valdivieso et al., 2014; Garrido et al., 2016).

Based on the visual aspect, PC2 is the component which seems to provide the best detection of defective areas in oranges. Thus, based on the loading plot obtained for this PC, the two most powerful spectral bands (679 and 755 nm) in PC2 were selected.

The resultant band ratio ($R_{\lambda 679}$/ $R_{\lambda 755}$) was applied to the reflectance images, with which the contrast between the sound surface and defects was more noticeable. After the application of the mask, the threshold was established to isolate the defective surface.

However, given the high level of heterogeneity present in the samples, when the validation of the model was carried out, the threshold value with which the highest accuracy was reached was not the same for all the samples. As a result, to find an optimal threshold value for separating sound from defective areas in oranges, the classification accuracy was calculated with threshold values within the range 0.23–0.35 in an increment of 0.02.

Fig. 7 shows the classification accuracy as a function of the threshold value established. After analysing the results shown in Fig. 7, it can be concluded that the highest accuracy (92.93% of the correctly classified pixels) was reached with a threshold value of 0.35. These results were similar to those obtained by Li et al. (2011), who selected bands 630 and 687 nm by analysing the principal components to detect 9 types of defects in 'Navel' oranges, and, after applying the ratio, obtained a precision of 98.2% in terms of correctly classified pixels.

To discriminate between defective and sound areas using the SWIR system, the optimal wavebands were investigated using the same methodology used with the Vis/NIR system. Thus, from the loading plot for PC2, the 1206 and 1518 nm wavebands were selected, which are related with C–H y O–H absorptions, respectively (Williams, 2001). The ratio image ($R_{\lambda1206}$/ $R_{\lambda1518}$) was created, using 1206 nm and 1518 nm images.

According to Fig. 7, which shows the accuracy obtained for each threshold value, the threshold value that yielded the best classification accuracy (89.31%) for the validation set was 0.29.

For this second objective, the difference in the accuracy obtained by both systems was not as great as in the differentiation between green leaves and oranges, and, the Vis/NIR system enabled to obtain the model with the greatest accuracy.

4. Conclusions

The results obtained in this study indicate the feasibility of using HSI technology to measure crop yield in oranges. The HSI systems can also potentially be developed further as a low-cost multi-spectral imaging system using the key wavelengths identified with the PCA method together with a simple ANOVA analysis from the calibration sets. Four wavelengths (679, 698, 755 and 951 nm) could potentially be implemented as MSI systems to differentiate green oranges from leaves and to detect orange peel defects, respectively, in the Vis/NIR system, and four wavelengths (1165, 1206, 1471 and 1518 nm) could also be used for the same purpose using the SWIR device.

For the two objectives proposed in this study (identification of fruits and detection of defects) in green orange, after using a two-band ratio coupled with a simple threshold method, a comparison of the two hyperspectral devices produced a better classification performance with the Vis/NIR system than with the SWIR system, with an accuracy of 96.97% when distinguishing between green oranges and leaves and an accuracy of 92.93% when detecting defects. Therefore, it could be concluded that Vis/NIR was the most suitable system for this application, with the added advantage of the equipment being more economical than the SWIR. However, it must be highlighted that the use of the polarizer with Vis/NIR system improved the signal reducing the specular reflection in samples, while for the SWIR system this accessory is not easily available. In addition, it must be added that if, as well as estimating the crop yield, certain chemical quality parameters in oranges also need to be measured simultaneously, it would be of great interest to incorporate a band related to the absorption of water or glucides, which would require the use of the spectral range of the SWIR system.

This work can be considered as a feasibility study and further studies are needed for in field application of these systems. In this study samples were measured in laboratory conditions using halogen lights and for remote sensing, under sun-light illumination, other factors must be taken into account.

Acknowledgements

This work was carried out under the bilateral (Spain-Republic of Korea) EUREKA R & D project entitled 'Development of ICT fusion smart farm technology for the intelligent production and distribution of oranges, INTELLIGENT-CITRUS'. The authors wish to express their gratitude to the Spanish Ministry of Education, Culture and Sports for the support offered to Irina Torres Rodríguez through the Training Programme for Academic Staff (FPU).

References

Arpaia, M.L., Kader, A.A., 1999. Orange. Recommendations for Maintaining Postharvest Quality. Perishables Handling #98. May. Postharvest Technology Center, University of California, Davis, USA.

Bulanon, D.M., Burks, T.F., Kim, D.G., Ritenour, M.A., 2013. Citrus black spot detection using hyperspectral image analysis. Agric. Eng. Int.: CIGR J. 15, 171–180. https://doi.org/10.3965/j.ijabe.20140706.004.

Cho, B., Kim, M.S., Baek, I.S., Kim, D.Y., Lee, W.H., Kim, J., Bae, H., Kim, Y.S., 2013. Detection of cuticle defects on cherry tomatoes using hyperspectral fluorescence imagery. Postharvest Biol. Technol. 76, 40–49. http://dx.doi.org/10.1016/j.postharvbio.2012.09.002.

Dale, L.M., Thewis, A., Boudry, C., Rotar, I., Dardenne, P., Baeten, V., Fernández-Pierna, J.A., 2013. Hyperspectral imaging applications in agriculture and agro-food product quality and safety control: A review. Appl. Spectrosc. Rev. 48, 142–159. https://doi.org/10.1080/05704928.2012.705800.

FAO, 2017. Citrus Fruit Fresh and Processed Statistical Bulletin 2016. Food and Agriculture Organization of The United Nations, Rome, Italy.

Garrido, Y., Tudela, J.A., Hernández, J.A., Gil, M.I., 2016. Modified atmosphere generated during storage under light conditions is the main factor responsible for the quality changes of baby spinach. Postharvest Biol. Technol. 114, 45–53. https://doi.org/10.1016/j.postharvbio.2015.12.001.

Garrido-Novell, C., Pérez-Marín, D.C., Amigo, J.M., Fernández-Novales, J., Guerrero, J.E., Garrido-Varo, A., 2012. Grading and color evolution of apples using RGB and hyperspectral imaging vision cameras. J. Food Eng. 113, 281–288. https://doi.org/10.1016/j.jfoodeng.2012.05.038.

Gowen, A.A., O'Donnell, C.P., Cullen, P.J., Downey, G., Frias, J.M., 2007. Hyperspectral imaging – an emerging process analytical tool for food quality and safety control. Trends Food Sci. Tech. 18, 590–598. https://doi.org/10.1016/j.tifs.2007.06.001.

Kane, K.E., Lee, W.S., 2007.Multispectral imaging for in-field green citrus identification. ASABE Paper No. 073025. ASABE, St. Joseph, MI, USA. https://doi.org/10.13031/2013.23169.

Keşan, G., Litvin, R., Bina, D., Durchan, M., Slouf, V., Polivka, T., 2016. Efficient light-harvesting using non-carbonyl carotenoids: Energy transfer dynamics in the VCP complex from *Nannochloropsis oceanica*. Biochim. Biophys. Acta Bioenerg. 1857, 370–379. https://doi.org/10.1016/j.bbabio.2015.12.011.

Kim, M.S., Chen, Y.R., Mehl, P.M., 2001. Hyperspectral reflectance and fluorescence imaging system for food quality and safety. T. ASAE 44, 721–729. https://doi.org/10.13031/2013.6099.

Kim, M.S., Chao, K., Chan, D.E., Jun, W., Lefcourt, A.M., Delwiche, S.R., Kang, S., Lee, K., 2011. Line-scan hyperspectral imaging platform for agro-food safety and quality evaluation: system enhancement and characterization. T. ASABE 54, 703–711. https://doi.org/10.13031/2013.36473.

Lee, K., Kang, S., Delwiche, S.R., Kim, M.S., Noh, S., 2008. Correlation analysis of hyperspectral imagery for multispectral wavelength selection for detection of defects on apples. Sens. Instrumen. Food Qual. 2, 90–96. https://doi.org/10.1007/s11694-008-9046-0.

Leemans, V., Destain, M.F., 2004. A real-time grading method of apples based on features extracted from defects. J. Food Eng. 61, 83–89. https://doi.org/10.1016/S0260-8774(03)00189-4.

Li, J., Rao, X., Ying, Y., 2011. Detection of common defects on oranges using hyperspectral reflectance imaging. Comput. Electron. Agric. 78, 38–48. https://doi.org/10.1016/j.compag.2011.05.010.

Li, J., Huang, W., Tian, X., Wang, C., Fan, S., Zhao, C., 2016. Fast detection and visualization of early decay in citrus using Vis-NIR hyperspectral imaging. Comput. Electron. Agric. 127, 582–592. https://doi.org/10.1016/j.compag.2016.07.016.

Li, X., Li, R., Wang, M., Liu, Y., Zhang, B., Zhou, J., 2018. Hyperspectral imaging and their applications in the nondestructive quality assessment of fruits and vegetables. In: Luna-Maldonado, A.L., Rodríguez-Fuentes, H., Vidales-Contreras, J.A. (Eds.), Hyperspectral Imaging in Agriculture, Food and Environment. IntechOpen Limited, London, UK, pp. 27–63. https://doi.org/10.5772/intechopen.72250.

Lorente, D., Blasco, J., Serrano, A.J., Soria-Olivas, E., Aleixos, N., Gómez-Sanchís, J., 2013. Comparison of ROC feature selection method for the detection of decay in citrus fruit using hyperspectral images. Food Bioprocess Technol. 6, 3613–3619. https://doi.org/10.1007/s11947-012-0951-1.

Martínez-Valdivieso, D., Font, R., Blanco-Díaz, M.T., Moreno-Rojas, J.M., Gómez, P., Alonso-Moraga, A., Del Río-Celestino, M., 2014. Application of near-infrared reflectance spectroscopy for predicting carotenoid content in summer squash fruit. Comput. Electron. Agric. 108, 71–79. http://dx.doi.org/10.1016/j.compag.2014.07.003.

Neter, J., Kutner, M.H., Nachtsheim, C.J., Wasserman, W., 1996. Applied Linear Statistical Models, fourth ed. McGraw-Hill, Columbus, USA.

Obenland, D., Collin, S., Mackey, B., Sievert, J., Fjeld, K., Arpaia, M.L., 2009 Determinants of flavour acceptability during the maturation of navel oranges, Postharvest Biol. Tecnol. 52, 156–163. https://doi.org/10.1016/j.postharvbio.2009.01.005.

Okamoto, H., Lee, W.S., 2009. Green citrus detection using hyperspectral imaging. Comput. Electron. Agric. 66, 201–208. https://doi.org/10.1016/j.compag.2009.02.004.

Porat, R., 2008. Degreening of citrus. Tree Forest. Sci. Biotechnol. 2, 71–76.

Vargas, A.M., Kim, M.S., Tao, Y., Lefcourt, A.M., Chen, Y.R., Luo, Y., Song, Y., Buchanan, R., 2005. Defection of fecal contamination on cantaloupes using hyperspectral fluorescence imagery. J. Food Sci. 70, 471–476. https://doi.org/10.1111/j.1365-2621.2005.tb11517.x.

Williams, P.C., 2001. Implementation of near-infrared technology. In: Williams, P.C., Norris, K.H. (Eds.), Near Infrared Technology in the Agricultural and Food Industries. AACC Inc., St. Paul, Minnesota, pp. 145–169.

Wise, B.M., Gallagher, N.B., Bro, R., Shaver, J.M., Windig, W., Koch, R.S., 2006. PLS_ToolBox 4.0. Manual for use with MATLAB (TM) [Computer software]. Eigenvector Research, Inc., Wenatchee, WA, USA.

Table 1

Details of the two hyperspectral cameras used.

Wavelength range	Vis/NIR (400–1000 nm)	SWIR (900–2500 nm)
Manufacture	Andor Technology (South Windsor, CT, USA)	Headwall Photonics (Fitchburg MA, USA)
Sensor	EMCCD	InGaAs
Bit depth	14 bits	12 bits
Spatial resolution	8 µm	24 µm
Number of bands	128	275
Spectral resolution	~ 4.7 nm	~ 6 nm
Illumination	Eight 100 W tungsten halogen lamps	Six 100 W tungsten halogen lamps
Exposure time	10 ms	50 ms

Fig. 1. Comprehensive flow for data analysis.

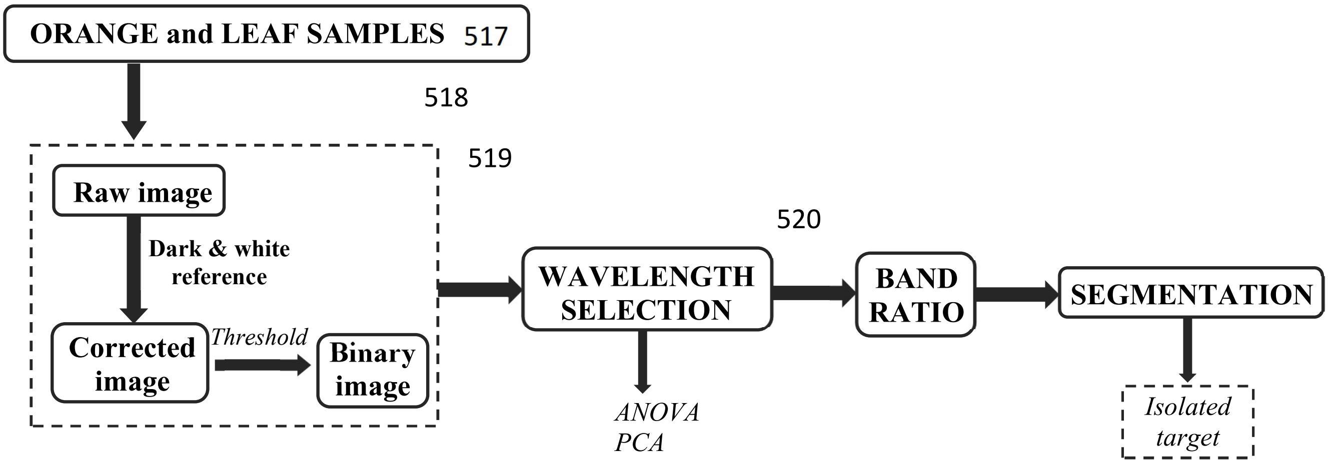

Fig. 2. Spectral features for leaves and green oranges obtained using the Vis/NIR (a) and SWIR (b) hyperspectral imaging systems.

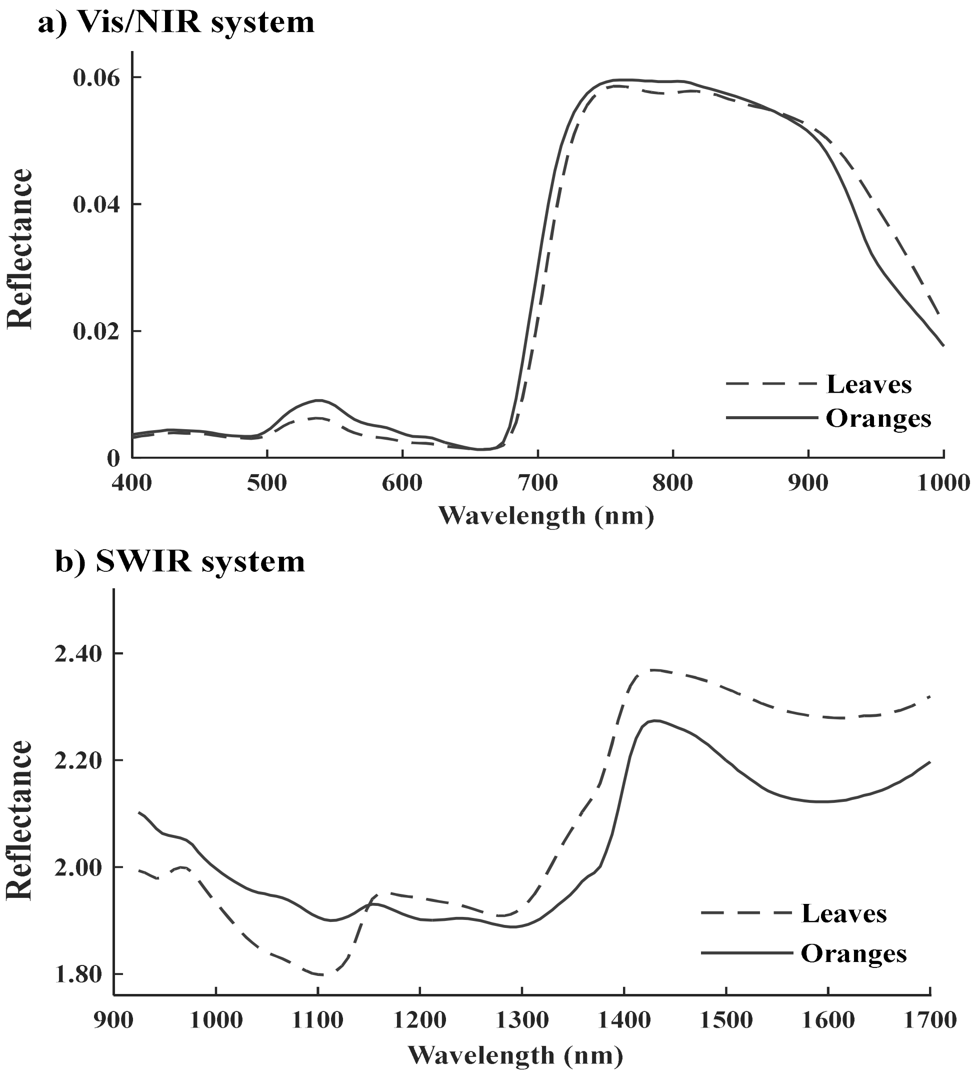

Fig. 3. F-values obtained for the distinction between green oranges and leaves using the Vis/NIR (a) and SWIR (b) hyperspectral imaging systems. Loading plots for the first three principal components for the Vis/NIR (c) and SWIR (d) data sets.

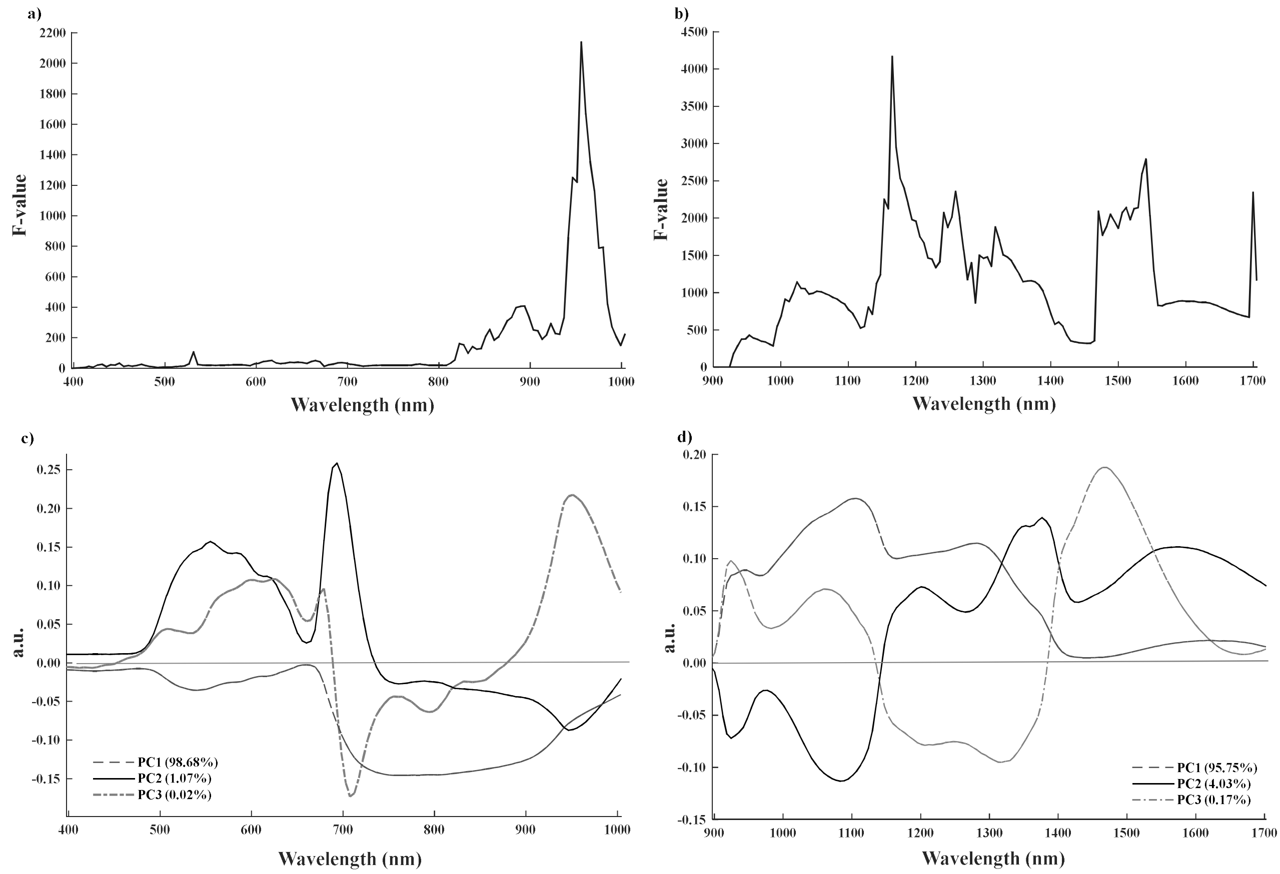

Fig. 4. (a) Reflectance image, (b) Binary image (mask), (c) Ratio image, (d) Histogram of frequencies.

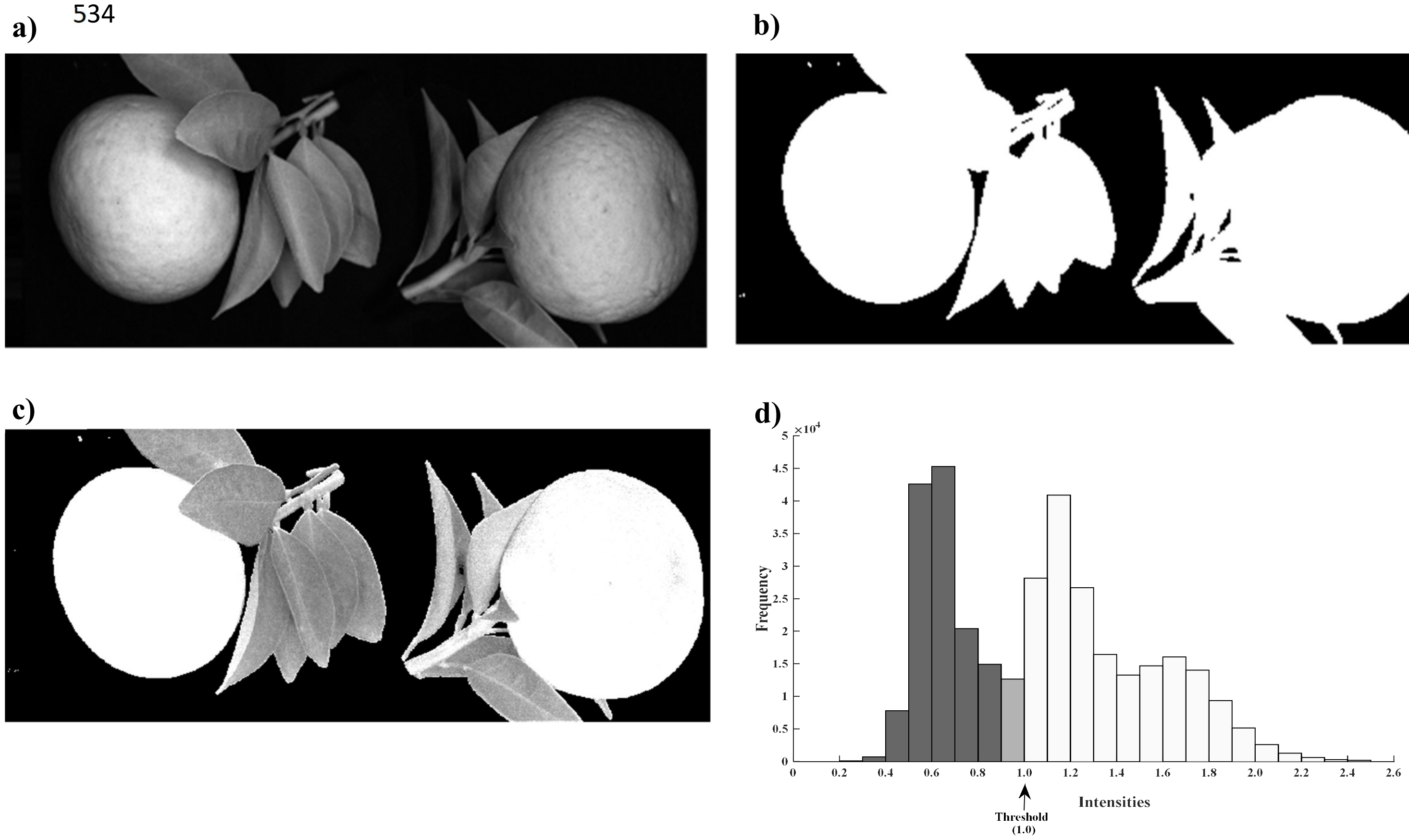

Fig. 5. Band ratio image ($R_{\lambda 1165}$/ $R_{\lambda 1471}$) for the differentiation between green oranges and leaves using the SWIR system.

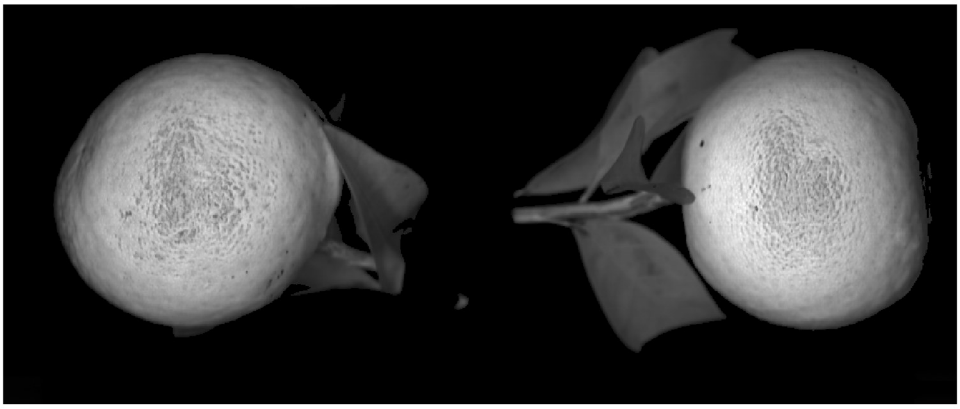

Fig. 6. PCA score images and loadings plot for the first three principal components using the Vis/NIR system.

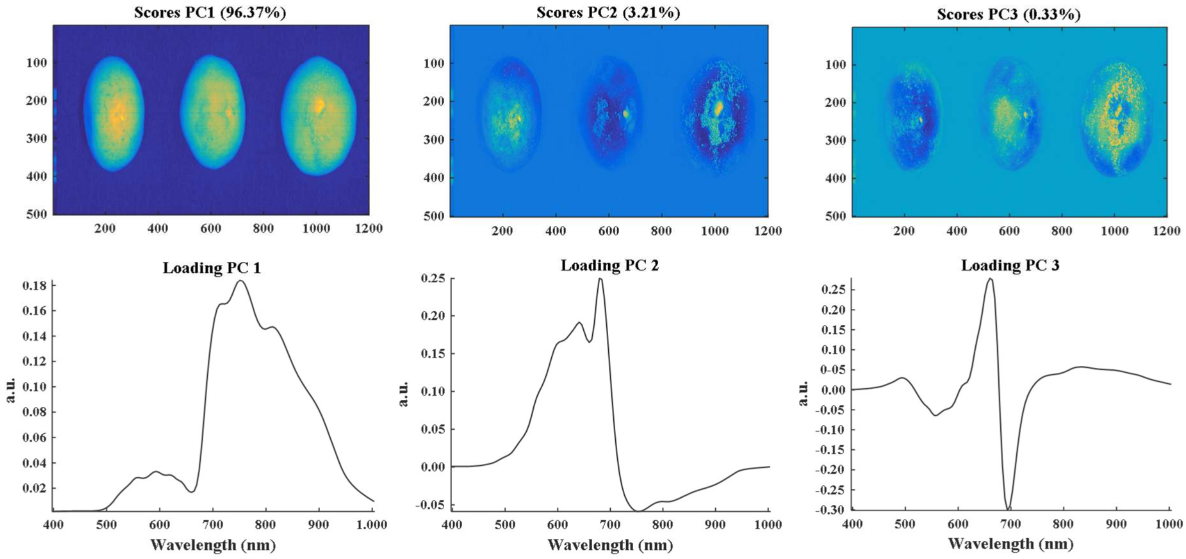

Fig. 7. Accuracy (%) for each threshold value applied using the Vis/NIR and SWIR based generated ratio images.